Approximate quantum mechanical method for describing excitations and related properties of finite single-walled carbon nanotubes

A. L. Montero-Alejo,[1,2] M. E. Fuentes,[3] E. Menéndez-Proupin,[4] W. Orellana,[5] C. F. Bunge,[6] L. A. Montero,[1] and J. M. García de la Vega[2]

[1]*Laboratorio de Química Computacional y Teórica, Facultad de Química, Universidad de la Habana, 10400 Havana, Cuba*
[2]*Departamento de Química Física Aplicada, Facultad de Ciencias, Universidad Autónoma de Madrid, 28049 Madrid, Spain*
[3]*Laboratorio de Química Computacional, Universidad Autónoma de Chihuahua, 31000 Chihuahua, Mexico*
[4]*Departamento de Física, Facultad de Ciencias, Universidad de Chile, Las Palmeras 3425, 780-0024 Ñuñoa, Santiago, Chile*
[5]*Departamento de Ciencias Físicas, Universidad Andrés Bello, Av. República 220, 837-0134 Santiago, Chile*
[6]*Instituto de Física, Universidad Nacional Autónoma de México, México, 01000, Mexico*

(Received 18 September 2009; revised manuscript received 5 May 2010)

Optical properties of three kinds of zigzag (5,0), (13,0), and (9,0) single-walled carbon nanotubes (SWCNTs) are studied using an approximate quantum mechanical method named complete neglect of differential overlap, which distinguishes basis atomic orbitals with different azimuthal l quantum numbers (CNDOL). This method models the electron energy transitions and excited state charge distributions through a configuration interaction of singly (CIS) excited determinants allowing the direct understanding of properties related with the total electronic wave function of nanoscopic systems, projecting a reliable quantum mechanical understanding to real life objects. The finite SWCNT's structures were obtained by replicating the unit cells of periodic SWCNTs and saturating the edge dangling bonds with hydrogens. The unit cell was previously relaxed using standard density functional theory methods. The behavior of these SWCNTs were interpreted in the framework of the CNDOL scheme by increasing the lengths of the tubes above 3 nm. As the nanotubes grow in length, the position of excited states for each SWCNT evolve differently: in contrast with (9,0) SWCNT, which exhibits favorable conditions for photoexcitation, the (13,0) and (5,0) SWCNTs do not show a lowering of the lowest excited states. This behavior is discussed by taking into account electron—electron interactions as considered in the framework of the CIS procedure. Furthermore, the (13,0) and (5,0) SWCNTs present forbidden transitions for the lowest excitations and its first dipole-allowed transitions are at 0.9–1.0 and 1.4–1.6 eV, respectively. In contrast, (9,0) SWCNT allows excitations by photon at less than 0.4 eV as the length of the nanotube tends to infinite. Excitons appear more bounded, energetically and spatially, in the (13,0) than in the (9,0) and (5,0) SWCNTs.

DOI: XXXX PACS number(s): 71.15.Qe, 71.15.Mb, 71.20.Tx, 71.35.−y

I. INTRODUCTION

The need to explain and predict the relationships between structural and electronic properties in nanoscale systems has brought together aspects of synthesis, measurements of physicochemical properties, and, in particular, the selection and adaptation of the most suitable methods for proper theoretical modeling. Relatively large polyatomic systems such as carbon nanotubes (CNTs), in which the expected non regular arrangements of atoms require the study of irreducible models, are presented as challenging even for the most approximate algorithms. Such systems are not crystals where the low or nonexisting entropy allows fear modeling with periodic approaches. In this field, many and different quantum theoretical methods have been explored in order to find a suitable way for representing and predicting the physical nature of the observed phenomena.[1]

Single-walled carbon nanotubes (SWCNTs) are considered ideal models because they can be considered to behave as one-dimensional molecular systems. Nowadays, the density-functional theory (DFT) is the standard method for optimizing the geometry and obtaining the electronic properties of extended systems since it can incorporate periodic conditions to achieve infinite models of these systems with a relatively low-computational cost. DFT is also the most used algorithm for interpreting and predicting experimental results, such as the conducting/insulating character of materials, as well as vibrational, thermal, and mechanical properties.[2–5] Standard DFT methods fail to predict energy gaps in insulating and semiconducting materials, underestimating ~50% with respect to the experimental values. However, for CNTs, the DFT band gaps seem to agree with the experimental transitions energies. This indicates a possible cancellation of the DFT gap error with the exciton binding energies.

The advances in the measurements of the optical properties of these materials have been widely significant. Available experimental results provide optical absorption[6–8] and fluorescence spectra[9–12] of isolated (noninteracting) SWCNTs. These results provide an important information for further applications of these materials. Moreover, all these optical data have increased the continuing questioning of the fundaments for understanding the behavior of the nanotubes. High-level calculations considering many-electron interactions have shown that the standard theory of interband transitions is unable to explain optical measurements.[13,14]

Optical excitations in nanostructures are multielectron collective states that cannot be always interpreted as single particle transitions. Some research has been directed to explain their collective absorption capacity and redistribution

of energy upon excitations by photons.[15] In the same way, there are several works devoted to the theoretical calculations of excitons in SWCNTs (Refs. 1, 14, and 16) where the many-particle electron-electron (e-e) interactions, beyond the single particle approximation, have been considered essential to achieve reliability for the calculated results.[13,17] Many-particle e-e interactions arise from the matrix elements of electron excitations as obtained from the Hartree-Fock (HF) Hamiltonian.[18] These e-e interactions are the same as the electron-hole interactions, although the later concept is applied in the context of quasiparticle rather than HF states, as well as in model Hamiltonians.

The method of configuration interaction[18] (CI) is a post-HF procedure. The e-e terms are being expressed in terms of Coulomb and exchange integrals and modify simple energy differences between one-electron molecular states resulting from the HF self-consistent field calculation. After a subsequent diagonalization of the composite secular matrix built with all such HF excitations in diagonal and their interactions in non diagonal elements, it results in an optimized electronic wave function of the system. CI allows a correct description of all ground and excited electronic states and their energies in small molecules, although its applicability to large systems is frequently prevented because the huge dimension of the CI Hilbert space. For medium sized systems, the CI Hilbert space uses to be restricted to single-electron (CIS) and single-plus double-electron (CISD) excitations of the HF Hamiltonian. Exciton states can be described by the CIS method in first approximation, while biexcitons needs the CISD level. Hence, CIS of polyatomic systems can be considered a method to get optimized transition energies, electron-hole interactions and charge redistributions due to excitons originated upon light absorption.[1] Zhao *et al.*[19,20] used this methodology within a simple and elegant HF framework of the π electron approximation named as the Pariser-Parr-Pople (PPP) parametrized Hamiltonian[21–24] achieving a qualitative description of the excitons in conjugated polymers and SWCNTs.

On the other hand, and in order to calculate properties of extended nanomaterials it is necessary to use models large enough to yield the best estimation of its macroscopic behavior. Most of the research on nanoscale systems[1] emphasizes the importance of combining advanced experimental information[9,25] with theoretical models that can distinguish different atomic arrangements.[26–29] However, the size of the typical nanostructures frequently exceeds the capabilities of most of the computing frameworks. The actual developments are directly focused on the searching of reliable models by using either parametrized semiempirical approaches[30] or others that include periodicity.[31]

The essential advantage of using a molecular orbital (MO) approach consists in reaching a complete wave function of the system, albeit being approximate. It allows getting more information from the behavior of charge distributions and redistributions upon excitation of a nanoscopic system than those obtained with any periodic approximations. Such approaches frequently rests on one electron wave functions for managing excited states and disallows nonperiodic perturbations that are normal in real systems. Our procedure could allow predictions for long nanotubes, which can be modeled taking into account irregularities and even randomly adsorbed impurities. CNDOL Hamiltonians,[32,33] based on the neglect of differential overlap (NDO) of atomic orbital basis sets and considering their azimuthal l quantum number, are essentially an approximate HF methodology without *a posterior*" parameter adjustments that has proven to be reliable.[32,34] It allows modeling systems with a very large number of atoms. The ground state is obtained by the self-consistent-field (SCF) method like in standard HF implementations. The electronic excitations are obtained using the CIS methodology. The algorithm admits increasing the active space (or number of CIS determinants) to be large enough for granting the best variational optimization of excited states and to account for the huge number of excitations in nanostructures. This method has provided an adequate description of phenomena related with intermolecular charge transfers in Rhodopsin protein associated with human vision[32] and the interaction between the chromophore and aluminosilicates to explain the stability of the ancestral maya blue color.[34] The aim of this paper is to explore how CNDOL can describe the electronic and optical properties of carbon nanotubes.

Three zigzag SWCNTs with chiral numbers (n,m), where $n=5$, 9, and 13 and $m=0$, were chosen as our model systems. The (5,0), (9,0), and (13,0) SWCNTs have diameters of 4.0, 7.1, and 10.2 Å, respectively. According to early literature[35] in this field, SWCNT electronic properties can be predicted approximately by the energy-band-folding theory of graphene. That is, a zigzag nanotube is a metal when n is multiple of three or a semiconductor with a moderate band gap for other values of n.[36,37] However, recent studies demonstrate that only the semiconducting character of the (13,0) SWCNT is predicted by this rule. The (9,0) SWCNT shows a small band gap corresponding to semiconductor materials that has been verified by experimental[38] and high level theoretical calculations.[5] Moreover, the (5,0) zigzag structure is predicted to be metallic, based on DFT calculations and the Green's functions method known as GW (where G is the one-particle Green's function and W is the screened Coulomb interaction).[13] Optical measurements, as well as DFT and high level calculations, show that isolated (5,0) SWCNTs have no optically allowed transitions below around 1.3 eV.[8,13] The first allowed electron transitions for (13,0) SWCNT is predicted at 0.9 eV by a regression analysis of spectrofluorimetic data.[11] Despite missing unambiguous absorption data for (9,0) SWCNT, the diameter of this nanotube (0.7 nm) falls in the diameter range of carbon nanotubes produced experimentally by laser vaporization method in macroscopic amounts.[39]

Optical absorption spectra of these kind of SWCNTs were measured and the large absorption peaks for the mixture ratio between the metallic and semiconducting tubes were estimated according to the conducting character.[39] Indeed, it is necessary to continue modeling the electron properties of these systems as well as other complex nanoscopic systems. More information is essential in order to clarify the relation between the electronic transport properties and the photoexcitation capabilities of these systems. It acquires even more importance if we take into account the huge field of optical properties of nanotubes with defects, bended structures, and

also doping agents inside. In the present work, we are modeling the optical properties of these SWCNTs by the CNDOL approach to project the possibilities of this Hamiltonian to build a wave function of a nanoscopic system.

II. THEORETICAL AND COMPUTATIONAL DETAILS

DFT calculations on periodic SWCNTs were performed using a plane-wave pseudopotential scheme as implemented in QUANTUM-ESPRESSO.[40] Exchange and correlation parts of the electronic energy were calculated in the generalized gradient approximation (GGA) with the functional of Perdew-Burke-Ernzerhof (PBE).[41] The effects of core electrons and nuclei are included using Rabe-Rappe-Kaxiras-Joannopoulos ultrasoft pseudopotentials.[42] We used the pseudopotential C.pbe-rrkjus. UPF from the cited QUANTUM-ESPRESSO distribution. A plane-wave basis set has been used, with kinetic energy cutoffs of 30 and 200 Ry for the expansion of the wave functions and the charge density, respectively. The one-dimensional Brilluoin zone was sampled using uniform grids of 14 k points for (5,0) and (9,0) SWCNTs and 6 k points for (13,0) SWCNT. In order to avoid convergence problems in the "metallic" (5,0) and small gap (9,0) SWCNTs, the method of cold smearing[43] with a broadening parameter of 0.01 Ry was used. The selected cutoffs, k-point grid, and smearing scheme allow us to obtain energies, forces, and stress converging within 0.008 eV/atom, 0.05 eV/Å, and 0.5 kbar, respectively. The initial structures were relaxed using damped Beeman dynamics[44] for the atoms and the simulation cell. Cell dynamics has restricted to the periodic direction of the SWCNT and was determined by the Wentzcovitch extended Lagrangian[45] with mass parameter of 0.0001 amu/au^2. The supercell is 25 Å wide in nonperiodic directions, whereas in the periodic direction it was optimized at 4.25621 Å for the (5,0), 4.26356 Å for the (9,0), and 4.26450 Å for the (13,0) SWCNTs. The stress tensor components of the relaxed structures were smaller than 0.5 kbar, the interatomic forces were smaller than 1 mRy/bohr, and the total energies were converged within 10^{-5} Ry.

CNDOL can address the electronic structure on the grounds of a molecular like construction thus allowing the possibility to include nonperiodic structural features of real systems. The availability of a wave function of the whole system allows a consistent picture of charge displacements (charge transfers) and state energies, considering the explicit inclusion of electron interactions in the Hamiltonian. This method initially provides a set of MO, expressed as a linear combination of atomic orbitals (AOs) for the studied systems. Up to this point, this approximation gives ground-state wave functions considering that all electrons remain strictly at the lowest energy states. However, an uncertain description of the virtual or empty MOs arises during the HF wave function optimization by a variational procedure due to the null density matrix elements of these orbitals. By the way, it occurs in all one electron like approaches, like tight binding, Hückel molecular orbital, etc., as well as in iterative HF and DFT-like procedures. In addition, performing large scale CIS-CNDOL calculations allows modeling the electronic nature of the excitons in these SWCNTs. The Coulomb and exchange terms between the occupied and virtual MOs to give the singlet transition has been taken into account to construct the CIS matrix, according to the well-known formulas.[46]

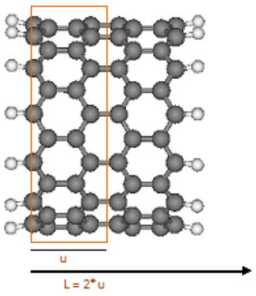

L	Length (nm)
2	0.71
4	1.56
6	2.42
8	3.27
10	4.12
12	4.98
14	5.83
16	6.68
18	7.54
20	8.39

FIG. 1. (Color online) Schematic representation of a (9,0,2) finite SWCNT. A table with the corresponding length in nanometres for each L value is shown in the box.

The CNDOL/21 Hamiltonian[32] has been used as described elsewhere. The NDOL2009 program version 6.6 (Ref. 47) was used and it is available from a website (http://karin.fq.uh.cu/~lmc/ndol/ndol2009-6.6.zip) for calculations of systems of up to 2000 atoms and 4500 basis orbitals. It can also provide electron densities of CIS excited states. The computed CIS transition energies always refer to singlet excitations regarding fixed and previously optimized geometries of the ground state. The oscillator strength is the output quantity that is proportional to the transition dipole between the excited and the ground state and indicates the intensity of photon absorptions.[48] Calculations can be performed in a reasonable computer time allowing applications to very big systems. The largest polyatomic system calculated in the present work for the (13,0) SWCNTs has 1066 atoms (1040 carbon atoms plus the edge hydrogens).

III. RESULTS AND DISCUSSION

We performed DFT calculations of band structures and density of states (DOS) of the three SWCNTs. They were evaluated for each unit cell obtained in the optimization. Based on the same level of the DFT approximation used for geometry relaxations we have obtained good agreement with previous published results.[5,13,49] (13,0) SWCNT is predicted as semiconductor with a moderate band gap of 0.62 eV. The (9,0) SWCNT energy gap predicted by this method is 0.11 eV. (5,0) SWCNT also appears as metallic in agreement with previous reports.[8,13]

We have studied about ten finite hydrogen-terminated SWCNTs for each chirality. Each one was constructed by replicating the unit cell (see Fig. 1) in even numbers between 2 and 20. SWCNT lengths ranged between 0.71 and 8.39 nm.

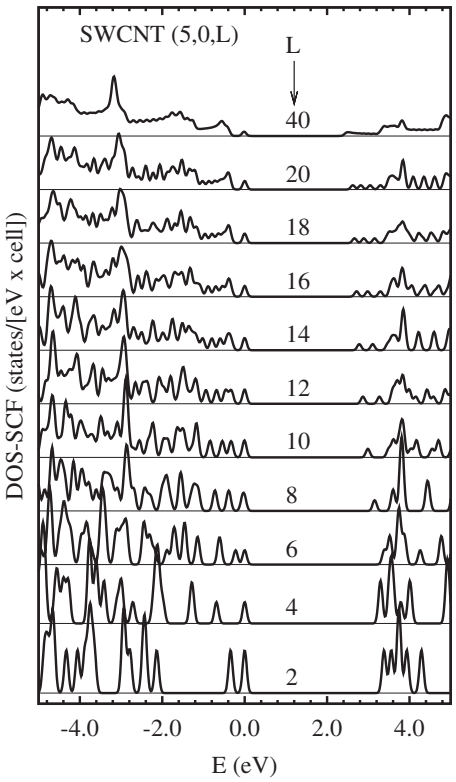

FIG. 2. Single particle DOS of $(5,0,L)$ SWCNT.

Finite SWCNTs were labeled as (n,m,L), following the notation of Hod and Scuseria,[50] where n and m are chiral numbers, and L is the number of units in each segment.

CNDOL results will be presented in the following order. Those for the (5,0) SWCNT are shown in Sec. III A. The discussion has been enhanced with experimental results of the optical spectrum. Likewise, the discussion will be extended to the (9,0) and (13,0) SWCNTs together in Sec. III B in order to provide a comparison between themselves.

A. (5,0) SWCNT

Most of the current quantum mechanical calculations in the field of periodic or quasiperiodic materials consider a simple MO scheme to be essential for studying the ground-state characteristics in the absence of external perturbations.[50] This kind of representation helps us to explore how long a finite nanotube model must be in order to obtain valid results for standard longer nanotubes. However, reliability of virtual orbitals is doubtful due to the limitations of the procedure, as mentioned above in the introduction to this paper. Figure 2 shows the single particle density of states per unit cell (DOS-SCF) i.e., related to MO's energies, of the (5,0,L) SWCNTs. The zero of energy scale is that of the highest occupied MO (HOMO). In this case, it was possible to extend the calculations to the model with $L=40$, which is 16.9 nm in length. In order to obtain soft curves, the sharp (deltalike) DOS was convoluted with a Gaussian distribution function with a width parameter of 0.05 eV (standard deviation). The shortest nanotube display isolated levels that are typical of molecular spectra. The picture also shows that the lowest unoccupied MO (LUMO) energy tends to decrease when the length increases. Increasing nanotube length yields the appearance of new peaks that finally coalesce in a quasi continuum spectrum. However, some peaks, like the one at 0 eV (HOMO together with other occupied orbitals close to it), remain isolated and show a trend to disappear. These peaks are due to "edge states," which remain constant in number, and get quenched when the DOS is divided by the number of unit cells. The picture shows that the (5,0,20) SWCNT, 8,4 nm in length, has a single particle DOS that roughly reproduces the converged DOS of long nanotubes. Gao *et al.*[31] studied finite nanotubes up to 100 nm long, showing that 20 nm SWCNTs display converged DOS and excluding the vanishing edge states.

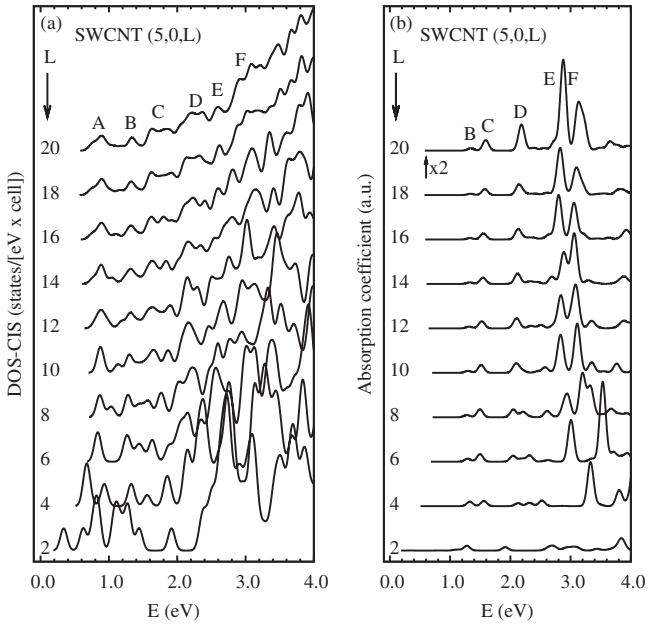

FIG. 3. Lowest energy excited states of $(5,0,L)$ SWCNT; (a) the density of states of CIS states and (b) the predicted absorption spectra between 0 and 4 eV. The absorption spectrum of $L=20$ has been multiplied by two times.

Figure 3 shows DOS electron excitations as calculated after the CIS treatment (DOS-CIS) of the series of (5,0,L) SWCNT and the corresponding optical absorption spectra (for nonpolarized light). Absorption spectra have been simulated by including Gaussian lineshape functions of 0.05 eV width multiplied by the oscillator strength of each electron excitation. The Gaussian broadening of DOS and absorption spectra represent our best estimation of the unknown energies in long nanotubes with respect to energies in small models. Spectra reveal irregular values of excitation energies in nanotubes shorter than about 3 nm, i.e., (5,0,8) SWCNT. It could be explained by taking into account the very molecule-like behavior of short length systems. The effect of the artificial edges breaking the C-C conjugate bonds may also play a role in such irregular behavior. Thus, these short length models will not be considered for the following analysis.

No significant changes appeared in energies of the excited states below 3.0 eV with an increase in length for model nanotubes. This behavior can be considered as a distinctive feature of this SWCNT. That is, its optical electron properties

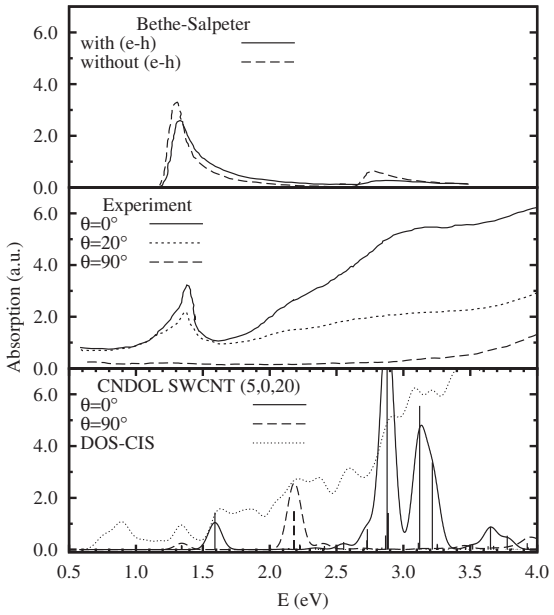

FIG. 4. Middle, experimental optical absorption spectra of SWCNT with diameter near 4 Å located in the pores of a zeolite. Top, calculated imaginary part of the dielectric function, obtained with the Bethe-Salpeter equation. Bottom, CNDOL absorption spectrum of (5,0,20) SWCNT. The electric field of light is polarized along the nanotube axis.

appear independent from the length of models when they are large enough. In order to describe the features of these excited states (below 3.0 eV) each maximum in DOS-CIS graph [Fig. 3(a)] has been indicated by a letter appearing at top of the largest SWCNTs. The lowest excited state (A) of the (5,0) SWCNT is optically forbidden as shown in Fig. 3(b). In contrast, the upper excited states enclosed in maxima from B to F, appear as allowed excitations due to their oscillator strengths. In particular, the large number of allowed electron transitions with high intensity, between 2.6 and 3.0 eV, gives rise to the appearance of a single maximum (E and F) in the calculated spectrum [Fig. 3(b)].

Figure 4 shows the experimental absorption spectra of a system of nanotubes inside the pores of a zeolite (Li *et al.*).[8] Pore diameters can only host SWCNT with chiralities (5,0), (3,3), and (4,2). The absorption was measured for polarized light at several θ angles with respect to the nanotube axis. For polarization that is perpendicular to the nanotube axes, the absorption is almost null. For polarization that is along the axis, there is a single peak at 1.37 eV with a shoulder at 1.19 eV. After 1.6 eV, one sees a continuum rising spectrum, where one can faithfully appreciate two broad bands centered at 2.1 and 3.1 eV. Above the experimental absorption representation, we see a plotting of the imaginary part of the dielectric function ε_2 calculated with the Bethe-Salpeter approximation by Spataru *et al.*[13] This spectrum corresponds to a polarization that is parallel to the nanotube axis. It shows one peak at approximately the same energy as the experiment, and a small band over 2.7 eV. The ratio of intensities should be different than that for the absorption coefficient, that is $\alpha=\omega\varepsilon_2/nc$, where ω is the light frequency, c is the velocity of light in vacuum, and n is the refraction index. Hence, in the absorption spectrum, the factor ω must cause a factor of 2 enhancement of the second band with respect to the first one, although this is modified by the energy dependence of the refraction index that we do not know. In the bottom of Fig. 4, we show the prediction of the CIS-CNDOL method. For parallel polarization, the spectrum has peaks at 1.34 (for B in Fig. 3) and 1.6 eV (for C in Fig. 3). These peaks may be assigned to the peak at 1.37 eV and the shoulder at 1.19 eV. There are two strong peaks at 2.88 (for F in Fig. 3) and 3.16 eV, produced by three strong transitions and a number of weak transitions. Notice that the peaks over 3.0 eV have not been assigned with letters in the Fig. 3, in order to gain clarity in the excitation spectra.

It seems clear that convolution curves of calculated excitations and the experimental spectrum cannot match exactly. Several effects are missing in both cases. One is the activation of many theoretically forbidden transitions due to phonons, defects, or by the crystal field produced by the surrounding zeolite pores where the spectrum is measured. That is the reason because we also show the DOS of all excited states found, which has a shape that resembles the optical absorption spectrum. The second possible cause is the effect of possible two-particle excitations, not considered neither in the CIS nor in the Bethe-Salpeter methods.

We also show the spectrum for perpendicular polarization. It only shows a peak at 2.18 eV (D in Fig. 3). It was not reported by Spataru *et al.*,[13] based on a curious classical electrodynamics argument[51] about a depolarization effect that is able to quench the perpendicular electric fields. This effect should be obtained from the full quantum mechanical treatment without resorting to classical ideas. However, the CNDOL calculation predicts a considerable absorption line at 2.18 eV. We do not know whether the Bethe-Salpeter calculation predicts absorption with perpendicular polarization. The fact that the experiment does not really show absorption in the case of perpendicular polarization, may indicate that the depolarization effect is produced by the dielectric properties of the pore walls surrounding the nanotube.

Different authors emphasize the interesting finite-size quantum effects of the energy gap of the carbon nanotubes because these materials are obtained experimentally as finite with an average length of several hundred nanometers.[31] To extrapolate our results to infinite nanotubes, we performed a linear regression of CIS energies (maxima A–F in Fig. 3) as functions of the inverse of nanotube lengths $(1/L)$ (Fig. 5). We prefer a qualitative assignment by only differencing the strongest allowed (s), the forbidden (f), medium (m), and weak (w) transitions. As expected, the slopes obtained from regression are close to zero, showing almost no dependence of the CIS energies from the model length. All regressions present a high linear correlation. The limit of these functions for large nanotube lengths (L) corresponds in each case with the value of the intercept. An inspection of these extrapolated values allows us to consider that a very long (5,0) SWCNT could show their first excitations at 1.38, 1.64, 2.24, 2.55, and 2.81 eV.

A qualitative explanation of these CNDOL results can be deduced after exploring the nature of each electron transition by means of the wave function probability amplitudes (the squared coefficients of basis set orbitals in the wave function

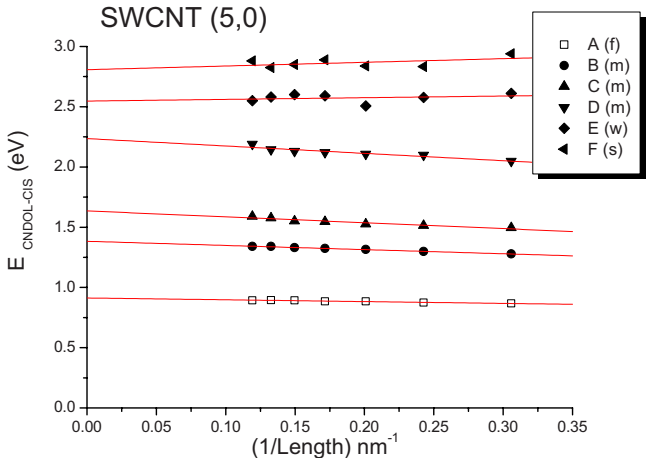

FIG. 5. (Color online) (5,0) SWCNT singlet state energies as a function of the inverse length of the system. Letters *f*, *s*, *m*, and *w* indicate forbidden, strong, medium and weak transitions, respectively.

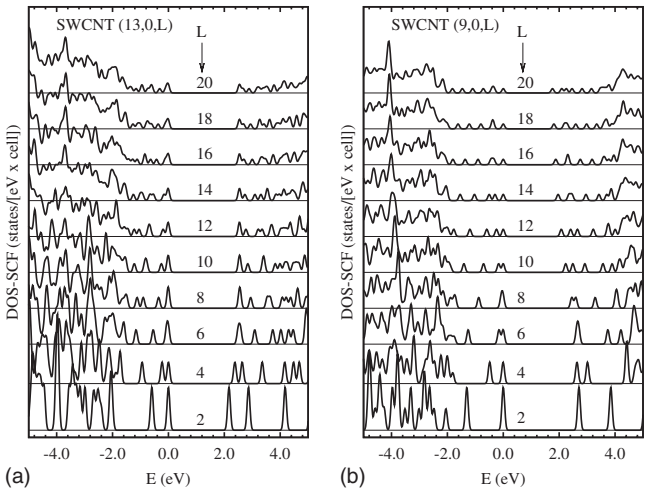

FIG. 6. Single particle densities of states of $(9,0,L)$ (on the left) and $(13,0,L)$ SWCNTs (on the right).

expansion). Thus, we can infer the corresponding distribution of excitons. Table I shows energies of excited states (indicated by a letter) and their corresponding oscillator strengths for the longest model i.e., (5,0,20) SWCNT. It is important to notice that only the energies of represented CIS state maxima [Fig. 3(b)] are shown graphically for the sake of clarity. All topologies of the omitted states are equivalent to those represented in the table. Schematic representations of MOs that show the largest contributions to each CIS transition are displayed at the bottom row of that table. Letters "occ" in green denotes in all cases the zone in the nanotube where is localized the occupied MOs responsible of the charge donation upon electronic transition. The zone of the empty MOs that should accept the charge appears as "unocc" in red. HOMOs and LUMOs are also highlighted when they are involved.

TABLE I. (Color online) Qualitative representation of the MOs for the (5,0,20) SWCNT.

Maximum DOS-CIS	*E* (eV)	Int	CIS model
A	0.89	*f*	I
B	1.34	*m*	I, II
C	1.59	*m*	I, III
D	2.19	*m*	I
E	2.55	*w*	I
F	2.88	*s*	I

Letters *f*, *s*, *m*, and *w* indicate forbidden, strong, medium, and weak transitions, respectively. Each type of CIS transitions is represented by I, II, and III.

Represented CIS model

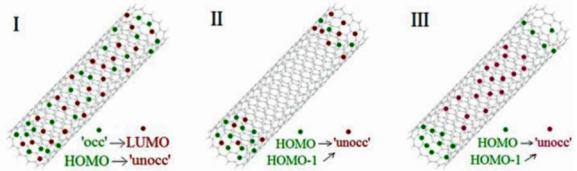

Curiously, the first forbidden CIS states of (5,0,20) SWCNT that is included in the "A" band, are mostly described as transitions between occupied and virtual MOs that are both delocalized throughout the nanotube. It includes the LUMO and other unoccupied MOs that are close in energy. HOMO and HOMO-1 MOs also appear in these transitions, but in such case the orbitals are localized at an extreme of the tube edge (without participation of ending H atoms). These results are consistent with those previously obtained[52] for finite graphene ribbons, where hydrogen atoms have also been used to saturate the edges. Indeed, this edge effect appears only related to the π topology of zigzag type structures, either in graphene ribbons or in semiconducting SWCNT.[3] The authors in that paper[52] claim that this interesting feature has a great significance in nanoscale materials, and it is expected that this "edge localized" states may play an important role in interfacing either between different carbon nanotubes or with another molecular systems.

It is important to notice that the first two allowed electron transitions and the degenerate CIS states ($\Delta E < 0.05$ eV) included in the B and C maxima are mainly described as charge transfers between MOs localized at the extremes, although they are scattered on both sides of the nanotube. In general, as it is shown in the picture of this table, the CIS model type I transitions are predominant for all the described CIS states. Thus, the charge transfer could be seen throughout the section of the (5,0) SWCNT that is independent from length.

B. (9,0) and (13.0) SWCNT's

Figure 6 shows the single particle density of states per unit cell (DOS-SCF) of both (9,0) and (13,0) nanotubes. Pictures illustrate that (9,0,20) and (13,0,20) SWCNTs, being 8.4 nm in length, show single particle DOS that generally

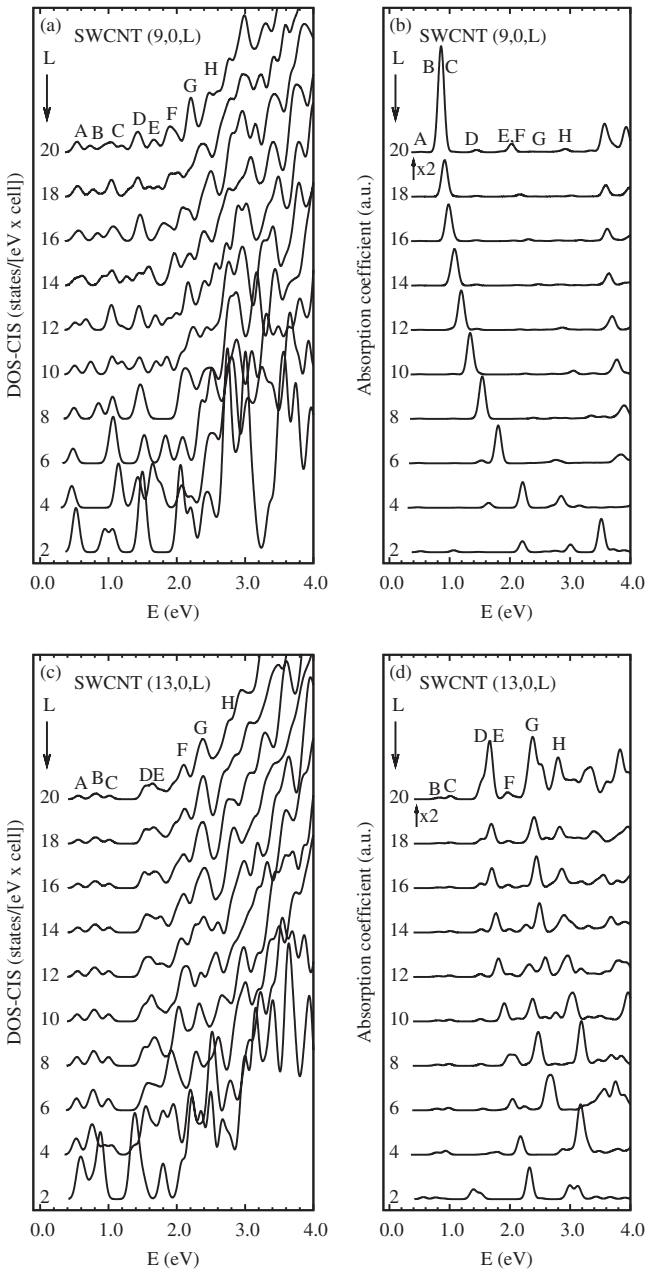

FIG. 7. Lowest energy excited states of $(9,0,L)$ (in a and b) and $(13,0,L)$ (in c and d) SWCNTs; density of states of CIS states (a and c), and predicted spectra (b and d) between 0 and 4 eV. In both SWCNTs, the absorption spectra of $L=20$ has been multiplied by two times.

converges to a unique pattern for each one when length increases. However, in both cases the peaks corresponding to the occupied states near to 0 eV tend to remain isolated. Furthermore, in the case of (9,0) models, the picture shows a clear reduction of the HOMO-LUMO energy gap (ΔE_{HL}) when the length increases, whereas it remains stable in the case of (13,0) SWCNTs. It must be noticed that, similar to the DOS-SCF representation of the (5,0) SWCNT, the origin of the decrease in the ΔE_{HL} values in (9,0) SWCNT comes from lowering the LUMO energies.

Figure 7 shows the electron excitation DOS obtained after the CIS procedure (DOS-CIS) and the corresponding simulation of optical absorption spectra (for non polarized light) of these nanotubes. Once again, the spectra reveal irregular values of excitation energies in nanotubes shorter than about 3 nm. However, the respective resulting patterns for the largest SWCNTs, together with those previously shown for the equivalent (5,0) models, can help us to explain their corresponding optical properties. In the case of (13,0,L) SWCNT do not appear significant changes in the lowest excited state energies below 1.5 eV while the model nanotube becomes longer, as seen above for $(5,0,L)$ SWCNT. However, the maxima in the predicted spectra, from E to H bands in Fig. 7, present a small red shift for larger nanotubes. This effect is also evident regarding the corresponding E, F, and G electron transition bands in the case of the (9,0) SWCNTs. Moreover, the B absorption maximum in this nanotube shows a significant redshift as its length increases. It exhibits optical properties that appear remarkably dependent on the size of the model.

As explained above, the only experimental data available to compare our results for the (9,0) SWCNT is that of absorption spectra for carbon nanotubes in the diameter range of 0.7 and 1.0 nm.[39] Kataura *et al.*[39] estimated that these nanotubes show a big absorption peak at 1.0 eV with a shoulder that produce a broad band. Moreover, a thinner peak with low intensity around 0.55 eV is also found in the spectra. There are other two low intensity peaks overlapped between 1.5 and 2.0 eV, but the authors consider that the absorption band at higher energies is not clearly defined. Our results are in agreement with all of these experimental observations [see Figs. 7(a) and 7(b) for the $(9,0,L)$ SWCNT]. It must be noticed that, for this nanotube, all of the CIS states are dipole allowed.

On the other hand, the lowest excited state (A) of $(13,0,L)$ SWCNT is optically forbidden [see Figs. 7(c) and 7(d)]. All analyzed upper excited states appear as allowed transitions as is denoted from their calculated oscillator strengths. This behavior has also been found for our result of the (5,0) and other zig-zag SWCNTs (Ref. 17) as obtained by HF-PPP method with a CIS scheme. Zhao and Mazumdar[17] highlighted the coincidence of the features of the spectra with those obtained for conjugated polymers. They even discuss the possibility that these systems could be quickly deactivated from their optically excited states to their low-energy forbidden state, instead of decaying directly to the ground state by emission of a photon.

Fluorescence measurements, in aqueous micellelike suspensions[9,10] of a wide range of semiconducting nanotubes, enabled to relate the structure and optical properties of this kind of materials.[11] Thus, the first and second optical transitions (interpreted as van Hove transitions) of the (13,0) SWCNT were empirically predicted at 0.9 and 1.8 eV.[11] As can be seen from the Fig. 7(d), the spectral features for large models obtained by CNDOL also predict the existence of these excitations. Notice that the B and C weak transitions are overlapped around 0.8 and 1.0 eV. The observed maximum must correspond to intense D, E and even to the small F peaks between 1.5 and 2.0 eV.

Figure 8 shows the linear regression study to extrapolate our results to infinite nanotubes. Again, all regressions

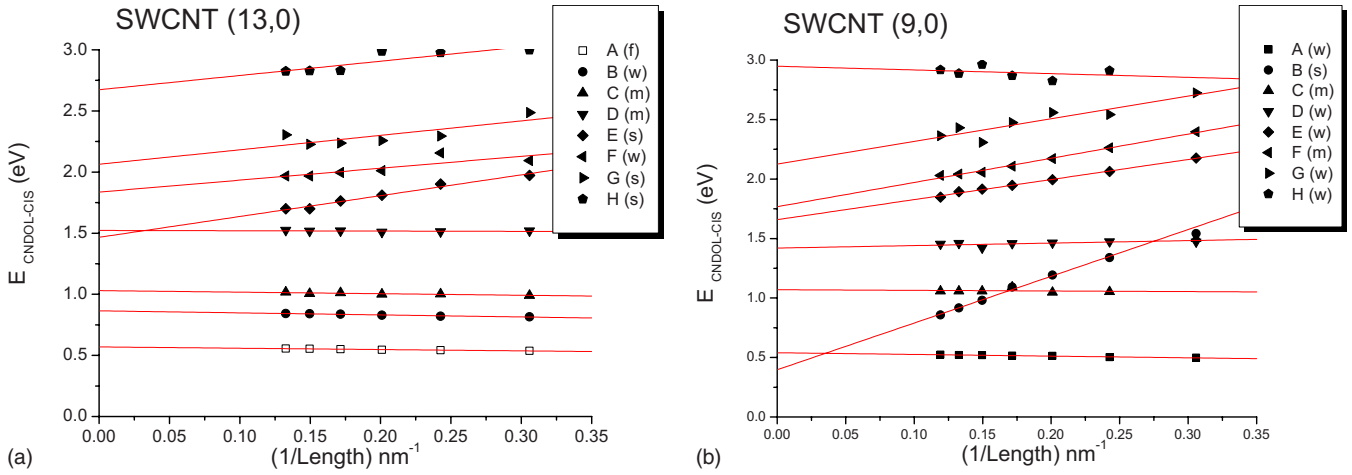

FIG. 8. (Color online) (9,0) and (13,0) SWCNTs singlet state energies as a function of the inverse length. Letters *f*, *s*, and *w* indicate forbidden, strong, and weak transitions, respectively.

present very good linear correlations. As expected, the slopes of the first excited states (up to about 1.5 eV) obtained from regression are close to zero in both SWCNTs, showing almost no dependence of the CIS energies on the length of the model. In contrast, the expected second excited state B [see Fig. 7(b)], of the (9,0) SWCNT's clearly shows a different behavior. This figure shows that SWCNT's lengths longer than 5 nm are needed to simulate this kind of structure with molecular approaches. Slightly negative slopes of the higher energy states in both nanotubes confirm the observed red shift of the spectrum. A simple inspection of these extrapolated values allows us to consider that the very long (13,0) SWCNTs could show first excitations at energies in the range of 0.86 and 1.03 eV, whereas long (9,0) SWCNTs only needs about 0.39 eV to be photoexcited.

Table II shows the energy, oscillator strength (related with the absorption intensity), and nature of each electron transition (indicated by a letter) for the two longest models: (9,0,20) and (13,0,20) SWCNTs. This qualitative explanation, by means of the CNDOL MOs with largest contributions to the CIS transitions, becomes essential for a better understanding of our results.

It is important to notice that the first weak electronic transition of (9,0,20) SWCNT appears to be near to size independent [band A in Figs. 7(a) and 7(b)], with values around 0.52 eV. However, and according to the above-mentioned extrapolation for large models, this is not the predicted lowest energy state that the system can reach at infinite lengths (Fig. 8). Then, the strong B state is the one found at lowest energy in long systems. It is mostly originated on a charge transfer that involves delocalized orbitals along the nanotube as a major contribution, including frontier orbitals (HOMO and LUMO). They are very size dependent, thus, it predicts that long (9,0) SWCNTs absorb a low energy photon in the infrared (0.4 eV $\sim$ 3200 cm^{-1}) and keeps alive the exciton due to a charge transfer process along the nanotube. According to the extrapolation, B needs a length that is longer than approximately 30 nm for becoming the lowest excitation in $(9,0,L)$ SWCNT.

The first forbidden CIS state [band A in Figs. 7(c) and 7(d)] of (13,0,20) SWCNT is mostly described as a transition between occupied and virtual MOs that are both localized on one side of the tube edge (without participation of ending H atoms). Thus, the charge transfer could be considered in a local section of the nanotube that is independent of the length. The upper allowed transitions of this SWCNT, from B to the strong E band, are mainly described as charge transfers between MOs being also localized at the extremes, although being scattered at both sides of the nanotube. Therefore, in the framework of our model all these transitions arise from excitations localized at nanotube edges. This picture differs from the traditional interpretation based on van Hove transitions in infinite edgeless nanotubes.[11] The longest $(13,0,L)$ nanotube that we calculated has 1040 carbon atoms, but its length is insufficient to sample van Hove singularities, as was done for the (5,0) SWCNT. Hence, further calculations are needed to clarify the importance of van Hove transitions on the optical properties of (13,0) SWCNTs. Nevertheless, the F, G, and H states, involve electronic transitions from and toward MOs delocalized over the entire nanotube.

Finally, we can infer and compare the corresponding distribution of the excitons taking into account the origin of the electron transitions which are represented in Table I and II for all of the studied SWCNTs. As described before, in the case of (9,0) SWCNTs the frontier MOs are delocalized wave functions along the tube axis. In fact, delocalization increases with the length while the gap ΔE_{HL} value decreases. The strong excitation B, which is fundamentally described as a charge transfer between these frontier MOs, and ΔE_{HL} are both correlated together. Thus, the difference between both values can be considered as the binding energy of the exciton associated to the HOMO-LUMO transition, which is stabilized by the e-e interaction.

The same feature is observed in case of (13,0) SWCNTs. The first allowed singlet transitions (B, C, and D) originate from MO's corresponding to the frontier peaks of the DOS scheme. However, in this case such peaks reflect the above described edge effect. Therefore, according to our approximation, neither ΔE_{HL} nor B, C, and D show size dependence on (13,0) SWCNT. Likewise, the favorable e-e interaction between these frontier MOs makes possible to find these CIS electronic excited states at lower energies.

TABLE II. (Color online) Qualitative representation of the MOs for long models of SWCNTs.

	SWCNT (9,0,20)			SWCNT (13,0,20)		
Maximum DOS-CIS	*E* (eV)	Int	CIS model	*E* (eV)	Int	CIS model
A	0.52	*w*	I, II	0.56	*f*	VI
B	0.86	*s*	I, III	0.84	*w*	II, VI
C	1.07	*m*	IV, I	1.02	*m*	VI
D	1.45	*w*	IV, V	1.52	*m*	II, VII
E	1.85	*w*	III, IV	1.70	*s*	II
F	2.03	*m*	I, IV, V	1.97	*w*	VIII
G	2.36	*w*	I, IV, V	2.31	*s*	VIII
H	2.92	*w*	I, IV, V	2.83	*s*	VIII

Letters *f*, *s*, and *w* indicate forbidden, strong, and weak transitions, respectively. Each type of CIS transitions is schematically represented by I, II, III, IV, V, VI, VII, and VIII.

Represented CIS model

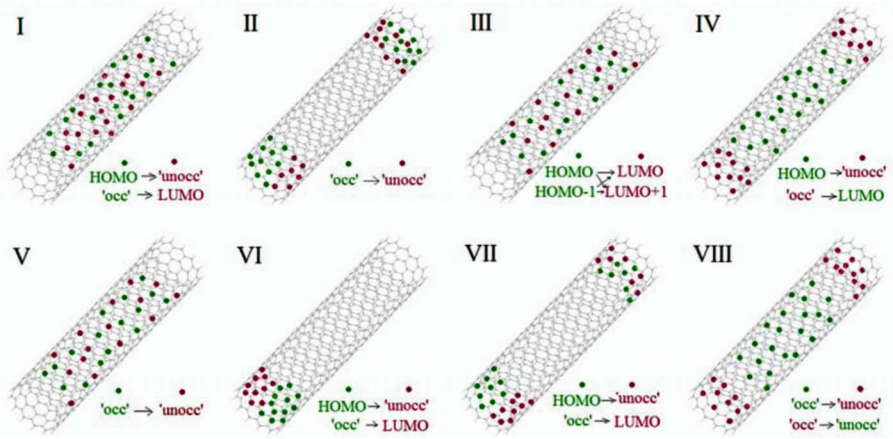

In contrast, (5,0) SWCNT analyzed in the Sec. III A, has the HOMO as an edge orbital, while the LUMO is delocalized along the tube axis. However, all first excited states below 3.0 eV, including those forbidden, are described with some degree of charge transfer contributions between delocalized MO's along the tube axis, including the edges. That is, excited states also include the assistance of the occupied ends of the second peak (at ~−0.5 eV) in the DOS-SCF scheme (Fig. 2), which correspond to the delocalized MOs. However, as previously shown, none of the excited states are size dependent. But both, the ΔE_{HL} gap and the energy difference between the second occupied peak and the LUMO, slightly decrease as the model length increases. The different size dependence of the B excitation and ΔE_{HL}, and the patterns shown in Table I, show that the B excitation cannot be regarded as an exciton associated to any predominant single-particle transition.

Figure 9 shows the dependence of ΔE_{HL} (gaps) and the lowest excited state on the model length for all the three SWCNT's. ΔE_{HL} for (9,0) and (13,0) SWCNT's behave in a similar way to that obtained for lowest excited states [see Figs. 9(a) and 9(b)]. However, this behavior changes for (5,0) SWCNT [Fig. 9(c)]. In the graph, the empty symbols represent ΔE_{HL} in each case, and they obviously appear at higher energies because electron interaction terms are not accounted, as they are *in CIS* states. Their electron interaction energies related to exciton binding (vertical dashed lines) show the relevance when CIS states are calculated for long SWCNTs. Clearly, this energy is higher for the (13,0) SWCNT than for the (9,0) SWCNT. In the case of (5,0) SWCNT, we could expect that the exciton binding energy will tend to converge at a low value as the length increases. The behavior of this property in different environments and other nanoscopic systems will be the object of a future work.

IV. CONCLUSIONS

Three kinds of SWCNT's with different expected optical behaviors and properties have been simulated by both DFT and CNDOL methods. DOS and band structures obtained for infinite SWCNTs by DFT method are in agreement with the

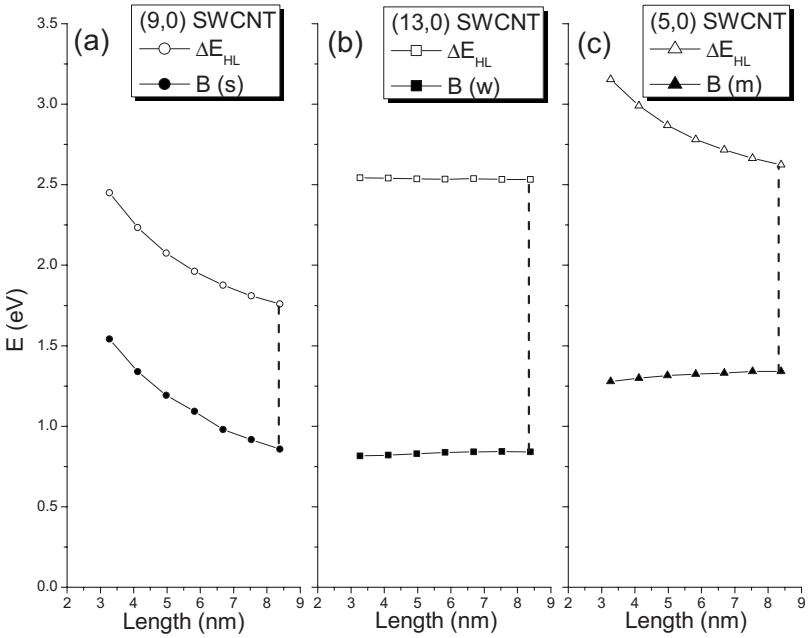

FIG. 9. Size dependence ΔE_{HL} and the lowest excited states.

expected results: the (13,0) SWCNT appears as semiconductor, the (9,0) as a small gap semiconductor and the (5,0) as metallic.

CNDOL calculations of the molecular electronic wave function were performed over a set of increasingly long, although finite, SWCNTs and then projecting the results to infinite lengths. It means to work with the electronic wave function of a nanoscopic system and opens the possibility to study non regular objects at that scale with reliable quantum mechanical tools.

Results show that it is important to consider finite models of SWCNT's longer than 3 nm in order to simulate realistic optical absorption properties corresponding to experimental scale systems. The excited states of the SWCNT's show different behaviors. (5,0) and (13,0) SWCNTs show the lowest excited state energies which are nearly independent of the SWCNT length. In contrast, the allowed excited state in (9,0) SWCNT tends to low the energy for longer nanotubes. Furthermore, (5,0) and (13,0) SWCNTs present forbidden transitions for the lowest CIS excited states. Their first dipole-allowed transitions are at 0.9–1.0 and 1.4–1.6 eV, respectively, showing no further significant changes for systems longer than 8 nm. However, (9,0) SWCNT appears to allow photon excitations at less than 0.4 eV as the length of the nanotube is tending to infinite.

All of these results are generally in agreement with the available experimental data. This correspondence permits us to predict other features of these optical properties. In the framework of our model, in the case of the (5,0) and (9,0) SWCNTs, the charge transfer could be seen throughout the section of the nanotube axis. However, the lowest electron transitions of the (13,0) SWCNT arise from excitations localized at nanotube edges. The importance of e-e interactions, which are related with the exciton bounding energy as given by the CIS calculations, was discussed for each SWCNT. Our results suggest that excitons are more bounded in the larger gap SWCNTs.

ACKNOWLEDGMENTS

Roald Hoffmann of Cornell University, Ithaca, NY, is gratefully acknowledged for useful comments and a revision of a preliminary version of the manuscript. Most of the authors are indebted to the Universidad de La Habana, Cuba, for the overall support of their education and work. The Universidad Autónoma de Madrid served as excellent host for the essential part of this work as well as the Spanish Agency for International Cooperation for Development (AECID) funding. The Deutsche Akademischer Austauchdienst (DAAD) provided part of the computational facilities in Havana. M.E.F. and the other authors are truly grateful for support from SEP-CONACYT (Grant No. 25380) of Mexico. E.M.-P. and W.O. thank support from PBCT-CONICYT (Chile) under Grants No. ACT/ADI-24 and No. ACI-52. J.M.G.V. is grateful for support from MEC of Spain (Grant No. CTQ 2007-63332) and AECID of Spain (Grant No. D/019558/08). L.A.M. is grateful to DFG's Forschergruppe 618 on Molecular Interactions for the kind support of part of his work on this matter. The CEAL (Banco Santander— UAM) project "Estados electrónicos de grafenos, nanotubos de carbono, fulerenos y nanocristales con posibles dopantes" inspired this work. Thanks to Jürgen Fabian as an inspirator of the presented method. T. Miyake is acknowledged for sharing his data of GW calculations.

[1] G. D. Scholes and G. Rumbles, Nature Mater. **5**, 683 (2006).
[2] U. Borstnik, M. Hodoscek, D. Janezic, and I. Lukovits, Chem. Phys. Lett. **411**, 384 (2005).
[3] F. Buonocore, F. Trani, D. Ninno, A. D. Matteo, G. Cantele, and G. Iadonisi, Nanotechnology **19**, 025711 (2008).
[4] C.-W. Chen and M.-H. Lee, Nanotechnology **15**, 480 (2004).
[5] T. Miyake and S. Saito, Phys. Rev. B **72**, 073404 (2005).
[6] M. Ichida, S. Mizuno, Y. Tani, Y. Saito, and A. Nakamura, J. Phys. Soc. Jpn. **68**, 3131 (1999).
[7] M. Ichida, S. Mizuno, Y. Saito, H. Kataura, Y. Achiba, and A. Nakamura, Phys. Rev. B **65**, 241407(R) (2002).
[8] Z. M. Li, Z. K. Tang, H. J. Liu, N. Wang, C. T. Chan, R. Saito, S. Okada, G. D. Li, J. S. Chen, N. Nagasawa, and S. Tsuda, Phys. Rev. Lett. **87**, 127401 (2001).
[9] S. M. Bachilo, M. S. Strano, C. Kittrell, R. H. Hauge, R. E. Smalley, and R. B. Weisman, Science **298**, 2361 (2002).
[10] M. J. O'Connell *et al.*, Science **297**, 593 (2002).
[11] R. B. Weisman and S. M. Bachilo, Nano Lett. **3**, 1235 (2003).
[12] F. Wang, G. Dukovic, L. E. Brus, and T. F. Heinz, Science **308**, 838 (2005).
[13] C. D. Spataru, S. Ismail-Beigi, L. X. Benedict, and S. G. Louie, Appl. Phys. A: Mater. Sci. Process. **78**, 1129 (2004).
[14] C. D. Spataru, S. Ismail-Beigi, L. X. Benedict, and S. G. Louie, Phys. Rev. Lett. **92**, 077402 (2004).
[15] Z. Wang, H. Pedrosa, T. Krauss, and T. Rothberg, Phys. Rev. Lett. **96**, 047403 (2006).
[16] G. D. Scholes, ACS Nano **2**, 523 (2008).
[17] H. Zhao and S. Mazumdar, Phys. Rev. Lett. **93**, 157402 (2004).
[18] A. Szabo and N. S. Ostlung, *Modern Quantum Chemistry: Introduction to Advanced Electronic Structure Theory* (Dover, New York, 1996).
[19] H. Zhao and S. Mazumdar, Synth. Met. **155**, 250 (2005).
[20] H. Zhao and S. Mazumdar, Phys. Rev. B **73**, 075403 (2006).
[21] J. A. Pople, Trans. Faraday Soc. **49**, 1375 (1953).
[22] R. Pariser and R. G. Parr, J. Chem. Phys. **21**, 466 (1953).
[23] R. Pariser, J. Chem. Phys. **21**, 568 (1953).
[24] R. Pariser and R. G. Parr, J. Chem. Phys. **21**, 767 (1953).
[25] V. V. Deshpande, B. Chandra, R. Caldwell, D. S. Novikov, J. Hone, and M. Bockrath, Science **323**, 106 (2009).
[26] L. Liu, C. S. Jayanthi, H. Guo, and S. Y. Wu, Phys. Rev. B **64**, 033414 (2001).
[27] W. Liang, X. J. Wang, S. Yokojima, and G. Chen, J. Am. Chem. Soc. **122**, 11129 (2000).
[28] W. Liang, S. Yokojima, D. Zhou, and G. Chen, J. Phys. Chem. A **104**, 2445 (2000).
[29] W. Liang, S. Yokojima, M.-F. Ng, G. Chen, and G. He, J. Am. Chem. Soc. **123**, 9830 (2001).
[30] A. Rochefort, D. R. Salahub, and P. Avouris, J. Phys. Chem. B **103**, 641 (1999).
[31] B. Gao, J. Jiang, Z. Wu, and Y. Luo, J. Chem. Phys. **128**, 084707 (2008).
[32] L. A. Montero-Cabrera, U. Röhrig, J. A. Padron-García, R. Crespo-Otero, A. L. Montero-Alejo, J. M. García de la Vega, M. Chergui, and U. Röthlisberger, J. Chem. Phys. **127**, 145102 (2007).
[33] L. A. Montero, L. Alfonso, J. R. Alvarez, and E. Perez, Int. J. Quantum Chem. **37**, 465 (1990).
[34] M. E. Fuentes, B. Peña, C. Contreras, A. L. Montero, R. Chianelli, M. Alvarado, R. Olivas, L. M. Rodriguez, H. Camacho, and L. A. Montero-Cabrera, Int. J. Quantum Chem. **108**, 1664 (2008).
[35] M. S. Dresselhaus, G. Dresselhaus, and R. Saito, Carbon **33**, 883 (1995).
[36] N. Hamada, S.-i. Sawada, and A. Oshiyama, Phys. Rev. Lett. **68**, 1579 (1992).
[37] R. Saito, M. Fujita, G. Dresselhaus, and M. S. Dresselhaus, Appl. Phys. Lett. **60**, 2204 (1992).
[38] M. Ouyang, J.-L. Huang, C. L. Cheung, and C. L. Lieber, Science **292**, 702 (2001).
[39] H. Kataura, Y. Kumazawa, Y. Maniwa, I. Umezu, S. Suzuki, Y. Ohtsuka, and Y. Achiba, Synth. Met. **103**, 2555 (1999).
[40] P. Giannozzi, Stefano Baroni, Nicola Bonini, Matteo Calandra, Roberto Car, Carlo Cavazzoni, Davide Ceresoli, Guido L. Chiarotti, Matteo Cococcioni, Ismaila Dabo, Andrea Dal Corso, Stefano de Gironcoli, Stefano Fabris, Guido Fratesi, Ralph Gebauer, Uwe Gerstmann, Christos Gougoussis, Anton Kokalj, Michele Lazzeri, Layla Martin-Samos, Nicola Marzari, Francesco Mauri, Riccardo Mazzarello, Stefano Paolini, Alfredo Pasquarello, Lorenzo Paulatto, Carlo Sbraccia, Sandro Scandolo, Gabriele Sclauzero, Ari P. Seitsonen, Alexander Smogunov, Paolo Umari, and Renata M. Wentzcovitch, J. Phys.: Condens. Matter **21**, 395502 (2009).
[41] J. P. Perdew, K. Burke, and M. Ernzerhof, Phys. Rev. Lett. **77**, 3865 (1996).
[42] A. M. Rappe, K. M. Rabe, E. Kaxiras, and J. D. Joannopoulos, Phys. Rev. B **41**, 1227 (1990).
[43] N. Marzari, D. Vanderbilt, A. De Vita, and M. C. Payne, Phys. Rev. Lett. **82**, 3296 (1999).
[44] D. Beeman, J. Comput. Phys. **20**, 130 (1976).
[45] R. M. Wentzcovitch, Phys. Rev. B **44**, 2358 (1991).
[46] L. A. Montero, L. A. Diaz, and N. Castillo, Chem. Phys. Lett. **364**, 176 (2002).
[47] L. A. Montero Cabrera, A. L. Montero Alejo, C. Bunge Molina, S. González Santana, R. Crespo Otero, and N. Mora Díez, NDOL2009: A computer program for calculation of approximate SCF-CI electron excitations and excited state properties of molecules with dynamic memory allocation, version 6.6, Universidad de La Habana and Universidad Autónoma de Madrid, Havana, 2009.
[48] R. Pariser, J. Chem. Phys. **24**, 250 (1956).
[49] W. Orellana and S. O. Vásquez, Phys. Rev. B **74**, 125419 (2006).
[50] O. Hod and G. E. Scuseria, ACS Nano **2**, 2243 (2008).
[51] H. Ajiki and T. Ando, Physica B **201**, 349 (1994).
[52] K. Nakada, M. Fujita, G. Dresselhaus, and M. S. Dresselhaus, Phys. Rev. B **54**, 17954 (1996).